Editors' Suggestion

Magnetoelectric spectroscopy of spin excitations in $LiCoPO_4$

V. Kocsis,[1,2] S. Bordács,[2,3] Y. Tokunaga,[1,4] J. Viirok,[5] L. Peedu,[5] T. Rõõm,[5] U. Nagel,[5] Y. Taguchi,[1] Y. Tokura,[1,6] and I. Kézsmárki[2,7]

[1]*RIKEN Center for Emergent Matter Science, Wako, Saitama 351-0198, Japan*
[2]*Department of Physics, Budapest University of Technology and Economics and MTA-BME Lendület Magneto-optical Spectroscopy Research Group, 1111 Budapest, Hungary*
[3]*Hungarian Academy of Sciences, Premium Postdoctor Program, 1051 Budapest, Hungary*
[4]*Department of Advanced Materials Science, University of Tokyo, Kashiwa 277-8561, Japan*
[5]*National Institute of Chemical Physics and Biophysics, Akadeemia tee 23, 12618, Tallinn, Estonia*
[6]*Department of Applied Physics and Tokyo College, University of Tokyo, Hongo, Tokyo 113-8656, Japan*
[7]*Experimental Physics 5, Center for Electronic Correlations and Magnetism, Institute of Physics, University of Augsburg, 86159 Augsburg, Germany*

(Received 25 July 2019; published 14 October 2019)

We have studied spin excitations in a single-domain crystal of antiferromagnetic $LiCoPO_4$ by terahertz absorption spectroscopy. By analyzing the selection rules and comparing the strengths of the absorption peaks in the different antiferromagnetic domains, we found electromagnons and magnetoelectric (ME) spin resonances in addition to conventional magnetic dipole active spin-wave excitations. Using the sum rule for the ME susceptibility, we determined the contribution of the spin excitations to all the different off-diagonal elements of the static ME susceptibility tensor in zero and finite magnetic fields. We conclude that the ME spin resonances are responsible for the static ME response of the bulk when the magnetic field is along the x axis, and the symmetric part of the ME tensor with zero diagonal elements dominates over the antisymmetric components.

DOI: 10.1103/PhysRevB.100.155124

I. INTRODUCTION

The magnetoelectric (ME) effect is the cross induction of polarization and magnetization by magnetic and electric field, respectively, as described by the ME tensor forms, $P_\mu = \chi_{\mu\nu} H_\nu$ and $\mu_0 M_\mu = \chi^{\mathrm{T}}_{\mu\nu} E_\nu$, where P_μ (M_μ) and H_ν (E_ν) are the $\mu, \nu = x, y, z$ components of the electric polarization (magnetic dipole moment) and the magnetic (electric) field. The ME effect is often associated with complex magnetic order parameters [1,2], such as the ferrotoroidal [3–8] and ferroquadrupolar moments [9], and magnetically induced chirality [10]. The ME effect provides a handle to manipulate these exotic spin orders and the corresponding magnetic domains even in the absence of spontaneous electric polarization or magnetization; thus, such ME materials have been proposed as building blocks for novel data storage and memory devices [11–13]. In some cases, such spin-multipolar orders have been revealed successfully by spherical neutron polarimetry [5,14] and x-ray spectroscopy [15] and investigated indirectly using static ME measurements [4,6,7,16] and second-harmonic generation microscopy [3,17,18].

In this work, we exploit a different approach to assign ferrotoroidal and ferroquadrupolar orders which is based on the measurement of the optical ME effect [8,19,20] using terahertz (THz) absorption spectroscopy. In a ME medium counterpropagating light beams can experience different indices of refraction, exhibiting optical directional anisotropy (ODA), as schematically shown in Fig. 1(b). This compelling phenomenon can be used to measure the dynamic ME response, also known as the optical ME effect, e.g., in resonance with magnon modes at THz frequencies. From the spectrum of the dynamic ME effect one can also determine the static ME coupling via the ME susceptibility sum rule [21]. Furthermore, THz absorption spectroscopy can measure the ME domain population as it has been successfully utilized to distinguish between the two types of antiferromagnetic (AFM) domains of $LiCoPO_4$ [13] [see Fig. 1(b)]. Here, in the case of $LiCoPO_4$, we demonstrate that the ODA can also be used to investigate the form and the spectral dependence of the ME susceptibility tensor and hence to identify different spin-multipolar orders responsible for the ME effect.

II. ADVANTAGE OF OPTICAL OVER STATIC ME EXPERIMENTS

When the ME phase appears upon a second-order phase transition from a high-temperature centrosymmetric and paramagnetic phase, the ME domains (α and β) connected by the spatial inversion and the time-reversal symmetries have ME susceptibilities of opposite signs, $\hat{\chi}^\alpha = -\hat{\chi}^\beta$. In the absence of electric (E) and magnetic (H) fields, a multidomain state is often realized, and the ME effect is canceled on the macroscopic scale. When a material possesses ferroelectricity or ferromagnetism, the P or M domain with an order parameter parallel to the conjugate electric (E^0) or magnetic (H^0) field is selected, respectively. However, when staggered electric and magnetic dipole orders or higher-order magnetic multipoles give rise to the ME effect, such direct control is not possible. Instead, a single ME domain can be selected by the simultaneous application of E^0 and H^0 fields upon cooling a sample

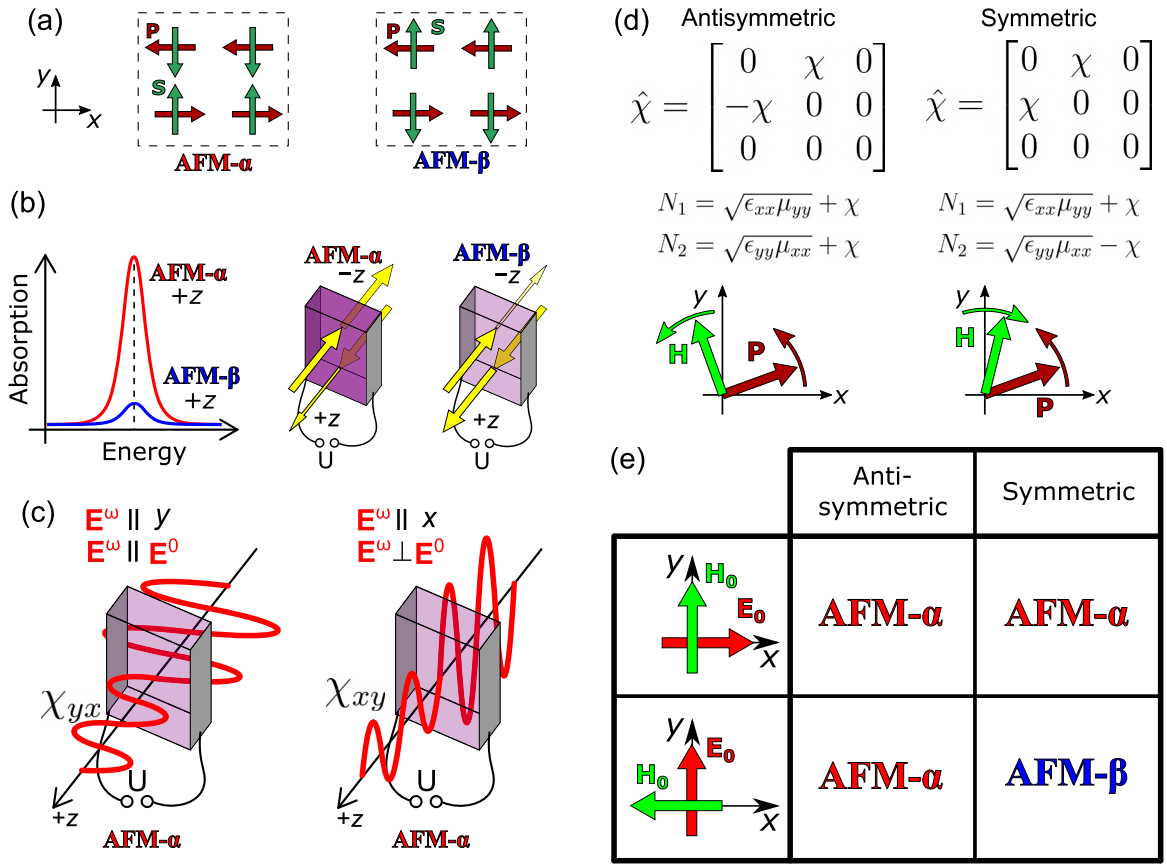

FIG. 1. (a) The two AFM domains of $LiCoPO_4$; AFM-α and AFM-β are characterized by ME coupling of opposite signs. (b) The dynamical magnetoelectric (ME) effect produces an absorption difference between light beams with the same polarizations propagating along the same directions ($+z$ or $-z$) in the two AFM domains. (c) Polarization of the probing light $\mathbf{E}^\omega$ can be selected either parallel or perpendicular to the poling electric field $\mathbf{E}^0$. Thus, in the dynamic ME measurement both elements of the ME susceptibility, χ_{xy} and χ_{yx}, can be simultaneously measured. (d) Electric polarizations and indices of refractions [Eqs. (1) and (2)] resulting from symmetric or antisymmetric ME susceptibility tensors ($\mathbf{P} = \hat{\chi}\mathbf{H}$) rotate against or together with the magnetic field, respectively. (e) For both the symmetric and antisymmetric forms of $\hat{\chi}$, the poling field combination $(+E_x^0, +H_y^0)$ selects the AFM-α domain. However, for the 90° rotated poling fields, poling with $(+E_y^0, -H_x^0)$ selects domain AFM-α or AFM-β in the case of antisymmetric and symmetric $\hat{\chi}$, respectively. This is because, with the former and latter forms of $\hat{\chi}$, the material couples to $E_x^0 H_y^0 \mp E_y^0 H_x^0$, respectively.

through the ordering temperature, which is often referred to as ME poling, while E^0 and H^0 are referred to as poling fields.

In general, the ME susceptibility tensor is the sum of a traceless symmetric part ($\hat{\chi}^{\mathrm{T}} = \hat{\chi}$, quadrupolar part), an antisymmetric part ($\hat{\chi}^{\mathrm{T}} = -\hat{\chi}$, toroidal part), and diagonal (axionlike) elements [2]. In order to visualize using a simple example how the magnetic-field-induced polarization varies with the orientation of the field, depending on the actual form of the ME tensor, we consider a system where the ME tensor has only two nonzero components, χ_{xy} and χ_{yx}. Correspondingly, the symmetric and antisymmetric parts of the ME tensor are given by $(\chi_{xy} + \chi_{yx})/2$ and $(\chi_{xy} - \chi_{yx})/2$, respectively. The symmetric and antisymmetric ME susceptibilities, often associated with quadrupolar and toroidal spin orders, respectively, behave differently upon the rotation of external fields in the xy plane, as shown in Fig. 1(d). If the magnetic-field-induced P is described by an antisymmetric ME susceptibility, it rotates in the same sense as H does, while it rotates in the opposite sense when generated by the symmetric, traceless ME susceptibility. Correspondingly, if the ME susceptibility tensor is fully antisymmetric, the selected domain depends only on the cross product of the poling E^0 and H^0 fields [see Fig. 1(e)]. Thus, poling with orthogonal E^0 and H^0 fields of certain orientation selects the *same* ME domain as poling with E^0 and H^0 fields mutually rotated by 90° in the xy plane. On the contrary, if the ME susceptibility tensor is symmetric and traceless, as shown in Fig. 1(d), the mutual rotation of E^0 and H^0 poling fields by 90° yields the selection of the *other* ME domain.

Static ME (P-H) measurements alone can usually provide limited information about the form of the ME susceptibility tensor. Since the same electric contacts are used to apply the E^0 poling field as well as to detect the magnetic-field-induced P, not all elements of the ME tensor can be measured in a single experimental configuration. More specifically, in a different experimental configuration where the E^0 poling field is perpendicular to the magnetic-field-induced P, it is difficult to perform a reliable measurement. In contrast, if the ME effect is detected optically via the ODA, the polarization of the probing light beam $\mathbf{E}^\omega$ can be chosen independently

of the poling field direction, either $\mathbf{E}^{\omega} \parallel \mathbf{E}^{0}$ or $\mathbf{E}^{\omega} \perp \mathbf{E}^{0}$, as illustrated in Fig. 1(c). Thus, both off-diagonal elements, χ_{xy} and χ_{yx}, can be measured optically for a given ME domain selected by the poling.

III. STATIC ME EFFECT OF $LiCoPO_4$

The paramagnetic phase of $LiCoPO_4$ is described by a centrosymmetric and orthorhombic space group (*Pnma*); that is, this material does not have any spontaneous electric polarization. The site symmetry of the magnetic Co^{2+} ions allows local electric dipoles in the xz plane, which are arranged in a staggered configuration on the four Co sites in the unit cell of this structure [13]. At $T_N = 21.3$ K a four-sublattice Néel-type AFM order emerges with $S = 3/2$ spins mainly coaligned along the y axis [22,23]. The two possible AFM domain states, α and β, which are also the two ME domains with opposite signs of $\hat{\chi}$, are illustrated in Fig. 1(a). In this compound, the Néel-type AFM order simultaneously breaks the inversion and the time-reversal symmetries, which allows finite χ_{xy} and χ_{yx} components of the ME tensor [4,24–26]. Although a small uniform canting of the spins may further reduce the magnetic symmetry and generate finite χ_{xz} and χ_{zx}, these weak secondary effects can be neglected in the present study [3,27]. Previously, the magnetically ordered state was identified as the first example of a ferrotoroidal order [3]; however, the form of the ME tensor, i.e., the relative sign of χ_{xy} and χ_{yx}, has remained an open question due to the experimental limitations discussed above [27].

We studied single-crystal $LiCoPO_4$ samples that were grown using the optical floating-zone method, similar to the procedure described in Ref. [28]. The ingots were aligned using a back-reflection Laue camera and cut into thin slabs with dimensions of $1 \times 5 \times 5\,\mathrm{mm}^3$. Static magnetization measurements up to $H = 140$ kOe were done using a physical property measurement system (PPMS, Quantum Design) equipped with a vibrating-sample magnetometer option. The magnetic-field-induced polarization measurements were carried out in a PPMS using an electrometer (6517A, Keithley) in the charge Q measurement mode.

Following the application of orthogonal poling fields ($\mathbf{E}^0 \parallel y$, $\mathbf{H}^0 \parallel x$) and ($\mathbf{E}^0 \parallel x$, $\mathbf{H}^0 \parallel y$), we measured the ME susceptibility as shown in Figs. 2(c) and 2(d), respectively. The experimental configurations are illustrated in Figs. 2(a) and 2(b), respectively. In both orientations, the measurement was carried out in all four different poling configurations, namely, with selectively reversed signs of the E^0 and H^0 fields. In the ordered phase $\mathbf{E}^0$ was switched off, and the displacement-current measurements were done in sweeping H field between ± 1 kOe five times. The magnitudes of the measured ME susceptibilities at $T = 2$ K are $|\chi_{xy}|/c = 15$ ps/m and $|\chi_{yx}|/c = 32$ ps/m and agree well with those previously reported in the literature [4]. Poling E^0 and H^0 fields of the same sign select one ME domain, while poling fields of opposite signs select the other ME domain [13]. However, due to the experimental limitations inherent in the static ME experiments as described above, only the absolute value of one of the two finite off-diagonal components of $\hat{\chi}$ can be measured for a given orientation of the poling fields. In contrast, if the ME effect is investigated optically, one can determine both χ_{xy} and χ_{yx} for each poled state, as will be discussed in detail in the following. This requires only the rotation of the light polarization by 90° in the plane of the poling fields.

IV. OPTICAL DETERMINATION OF THE ME SUSCEPTIBILITY TENSOR

Spin excitations with ME character, the ME resonances [8,29], can be simultaneously excited by the electric ($\mathbf{E}^{\omega}$) and magnetic ($\mathbf{H}^{\omega}$) components of light and therefore can be exploited to probe the elements of the dynamic ME susceptibility tensor. Such spin resonances can show a strong absorption difference for the respective ME domains due to the opposite signs of the ME susceptibility in the two domains, α and β. When light propagates in such a material, the oscillating magnetizations in both the α and β domains fluctuate in phase with $\mathbf{H}^{\omega}$, while the corresponding magnetically induced polarizations in the two domains oscillate in antiphase with respect to each other. As a result, the index of refraction for light propagation along the $+z$ axis of the crystal is different for the two domains [30,31]:

$$N_1^{\alpha/\beta}(\omega) = \sqrt{\epsilon_{xx}(\omega)\mu_{yy}(\omega)} + \chi_{xy}^{\alpha/\beta}(\omega) \tag{1}$$

for $\mathbf{E}^{\omega} \parallel x$, $\mathbf{H}^{\omega} \parallel y$, and

$$N_2^{\alpha/\beta}(\omega) = \sqrt{\epsilon_{yy}(\omega)\mu_{xx}(\omega)} - \chi_{yx}^{\alpha/\beta}(\omega) \tag{2}$$

for $\mathbf{E}^{\omega} \parallel y$, $\mathbf{H}^{\omega} \parallel x$, where $\epsilon_{\nu\nu}$ and $\mu_{\nu\nu}$ ($\nu = x, y$) are elements of the dielectric permittivity and magnetic permeability tensors, respectively. The light absorption is different for the two ME (AFM) domains as the ME susceptibility has opposite signs for them, $\hat{\chi}^{\alpha} = -\hat{\chi}^{\beta}$. We note that the reversal of the light propagation direction from $+z$ to $-z$ is equivalent to the exchange of the ME domains [Fig. 1(a)]; thus, the ODA also has opposite signs for the two ME domains. The sign difference between Eqs. (1) and (2) is related to the rotation of the light polarization. From Eqs. (1) and (2), it follows that in materials with an antisymmetric ME effect ($\chi_{xy} = -\chi_{yx}$) the differences in the refractive indices of the two AFM domains, $\Delta N_1 = (N_1^{\alpha} - N_1^{\beta})/2$ and $\Delta N_2 = (N_2^{\alpha} - N_2^{\beta})/2$, are the same for the two orthogonal light polarizations, $\Delta N_1 = \Delta N_2 = \chi_{xy}$. On the other hand, for systems with symmetric ME susceptibility tensor ($\chi_{xy} = \chi_{yx}$), the differences in the refractive indices of the two domains changes sign upon the rotation of light polarization by 90°, i.e., $\Delta N_1 = -\Delta N_2 = \chi_{xy}$. We note here that such changes in the ODA have to be probed on a single excitation, as the sign of the optical ME susceptibility is specific to the different excited states.

V. MAGNONS, ELECTROMAGNONS, AND ME RESONANCES IN $LiCoPO_4$

Optical absorption spectra of $LiCoPO_4$ were measured at the National Institute of Chemical Physics and Biophysics, Tallinn, using a Martin-Puplett interferometer combined with a superconducting magnet, applying magnetic fields up to $H = 170$ kOe. The relative absorption spectra recorded at $T = 5$ K, using linearly polarized light with $\mathbf{E}^{\omega} \parallel y$ and x, are shown in Figs. 2(e) and 2(f) and 2(g) and 2(h), respectively. The sample was cooled to a ME single-domain state in $E^0 = 1$ kV/cm and $H^0 = 1$ kOe poling fields, respectively, applied

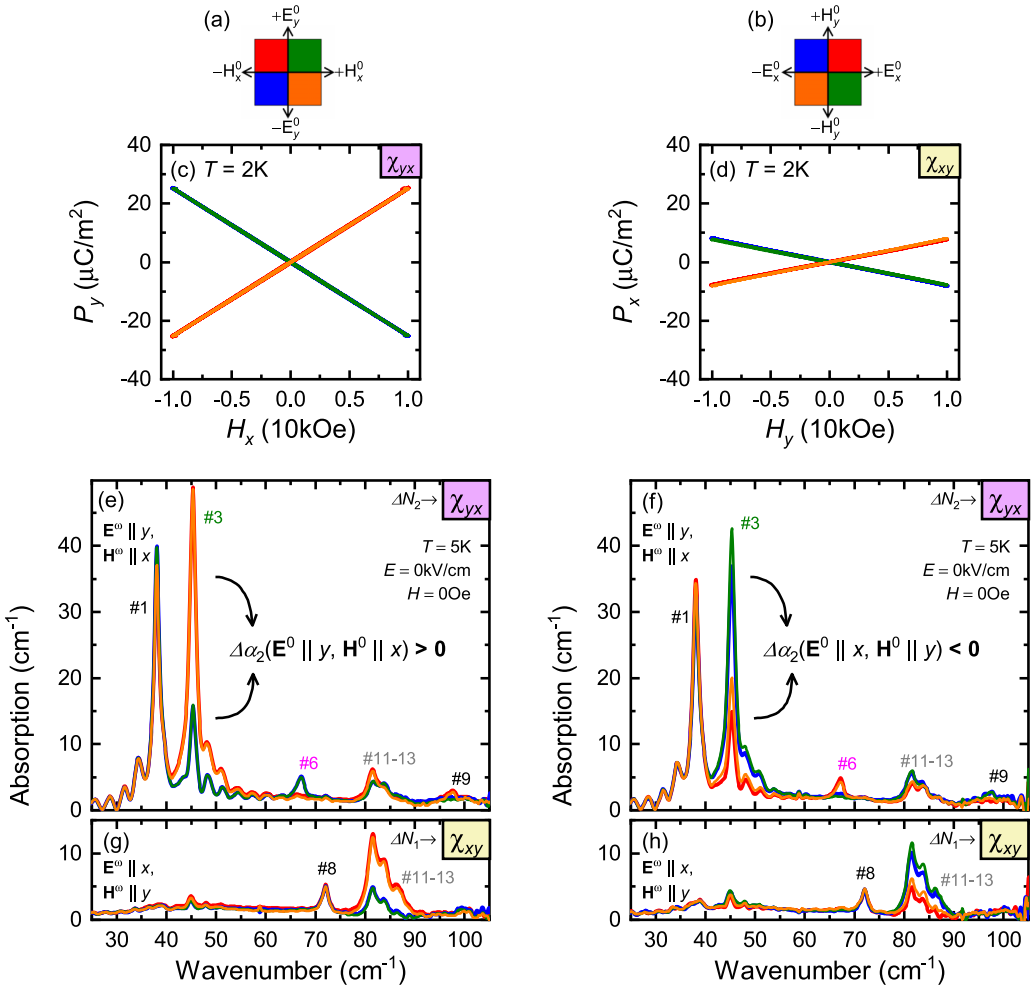

FIG. 2. Remanent static and dynamic ME effects in $LiCoPO_4$. (a) and (b) Experimental configuration of the $\mathbf{E}^0$ and $\mathbf{H}^0$ poling fields. The color code of (b) corresponds to the simultaneous 90° rotation of the fields of (a) [24]. (c) and (d) Poling field dependence of the *P*-*H* curves at $T = 5$ K for (c) $\mathbf{E}^0 \parallel y$ and $\mathbf{H}^0 \parallel x$ and (d) $\mathbf{E}^0 \parallel x$ and $\mathbf{H}^0 \parallel y$ poling field configurations. The color codes of (c) and (d) are shown in (a) and (b), respectively. The slopes of the *P*-*H* curves correspond to χ_{yx} and χ_{xy} in (c) and (d), respectively. The sign of the ME effect depends on the relative signs of the poling fields; note the complete overlap of the red and orange as well as the blue and green curves. (e)–(h) Optical absorption spectra measured at $T = 5$ K (e) and (g) with poling configurations indicated in (a) and (f) and (h) with poling configurations shown in (b). Spectra in (e) and (f) were measured using linearly polarized light with E_y^ω, H_x^ω, while those in (g,h) were measured with E_x^ω, H_y^ω. The spectra of the dynamic ME coefficients can be calculated as the absorption difference of the different domains, according to Eqs. (1) and (2). The $\Delta\alpha_2$ ODAs in (e) and (f) as well as in (g) and (h) change sign for the rotation of the poling E^0 and H^0 poling fields, according to Eqs. (3) and (4), respectively.

along the y and x axes. The low-temperature absorption measurements were carried out after switching off the poling fields. The relative absorption spectra were obtained by subtracting a reference spectrum taken in the paramagnetic phase, at $T = 30$ K [24]. Thus, the low-temperature spectral features are related to excitations emerging in the magnetically ordered state: Two strong (1 and 3) and several weaker (6, 8, 9, and 11–13) resonances appear in the AFM phase.

The poling-field-dependent resonances, 1, 3, 6, 9, and 11–13, are ME resonances since the ME response has opposite signs in the α and β domains. For the same signs of the poling fields, $(+E_y^0, +H_x^0)$ and $(-E_y^0, -H_x^0)$, modes 3, 9, and 11–13 have large absorptions, while for opposite signs of the poling fields, $(-E_y^0, +H_x^0)$ and $(+E_y^0, -H_x^0)$, the same modes show lower absorption. As the magnitude of the absorption difference for the ME domains is the highest for resonance 3, in the following we will focus on this mode. It appears when light polarization is $\mathbf{E}^\omega \parallel y$ and $\mathbf{H}^\omega \parallel x$; thus, according to Eq. (2), it probes $\chi_{yx}(\omega)$. For static poling fields $\mathbf{E}^0 \parallel y$ and $\mathbf{H}^0 \parallel x$ the difference of the absorption coefficients $\Delta\alpha = \frac{2\omega}{c}\mathrm{Im}(\Delta N)$ was found to be positive:

$$\Delta\alpha_2 = \left[\alpha_2\left(+E_y^0, -H_x^0\right) - \alpha_2\left(-E_y^0, -H_x^0\right)\right]/2 > 0, \quad (3)$$

which is clear from Fig. 2(e). On the other hand, for poling fields rotated by 90° to $\mathbf{E}^0 \parallel x$ and $\mathbf{H}^0 \parallel y$ the difference of the absorption coefficients changed sign:

$$\Delta\alpha_2 = \left[\alpha_2\left(+E_x^0, +H_y^0\right) - \alpha_2\left(-E_x^0, +H_y^0\right)\right]/2 < 0, \quad (4)$$

as seen in Fig. 2(f). From this we can conclude that if poling with $(+E_y^0, -H_x^0)$ and $(-E_y^0, -H_x^0)$ has selected domains α and β, respectively, then poling with $(+E_x^0, +H_y^0)$

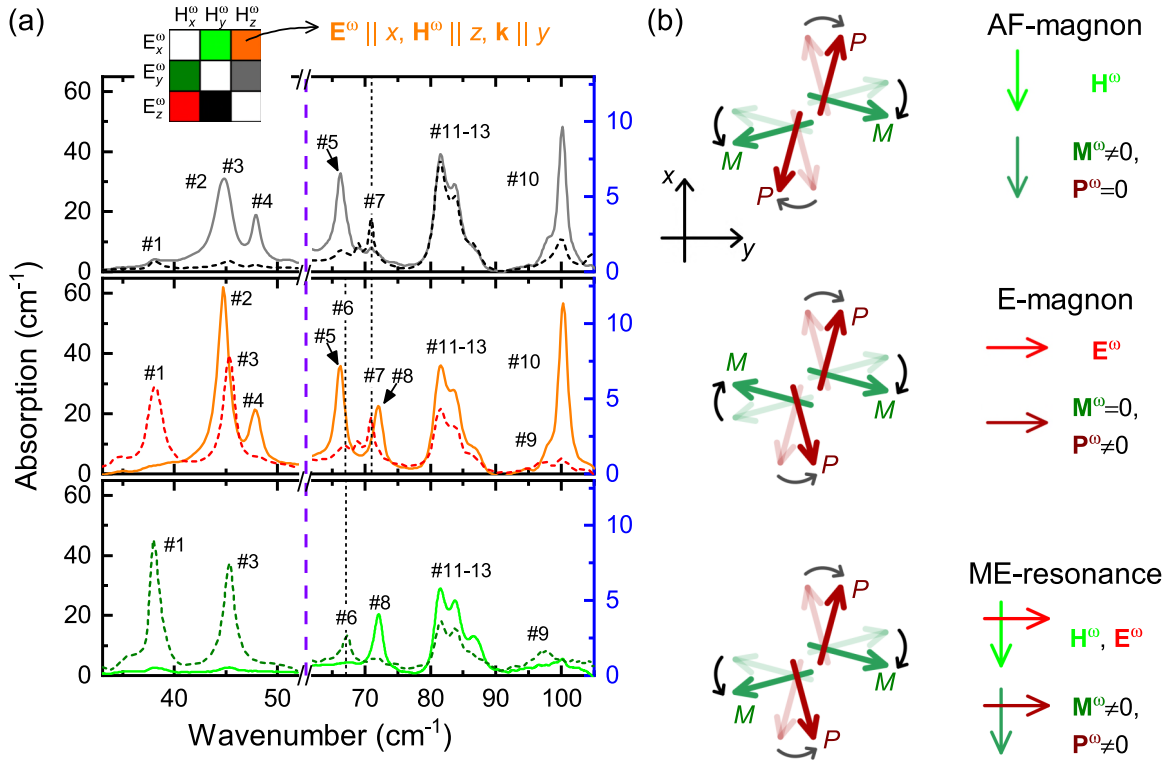

FIG. 3. (a) Optical absorption spectra, measured in six different configurations of $\mathbf{E}^\omega$ and $\mathbf{H}^\omega$ of the light at $T = 5$ K, revealing the selection rules of the magnetic excitations. The inset indicates the color code of the different light polarizations, along with an example where $\mathbf{E}^\omega \parallel x$, $\mathbf{H}^\omega \parallel z$, and $\mathbf{k} \parallel y$. Note the difference in the vertical scales corresponding to the spectral regions below and above the vertical dashed line. (b) Schematic illustration of an antiferromagnetic resonance (AF-magnon), an electromagnon (E-magnon), and a ME resonance. These modes are excited by only the magnetic component, by only the electric component, and simultaneously by both components of the electromagnetic radiation. For the sake of simplicity, we illustrate the excitations with one representative pair of spins M of the magnetic unit cell along with the respective local polarization P. The dynamic nature of the excitations is captured by curved arrows, which represent in-phase or antiphase oscillations of M and P. The net dynamic magnetization and polarization of the unit cell are labeled $\mathbf{M}^\omega$ and $\mathbf{P}^\omega$, respectively.

and $(-E_x^0, +H_y^0)$ must have selected domains β and α. It means that rotation of the poling fields by 90° results in the selection of the other ME domain, as illustrated in Fig. 1(e). As discussed in Sec. II and also visualized in Fig. 1(d), the selection of different ME domains by a 90° rotation of the poling fields implies that the symmetric traceless part of the ME tensor dominates over the antisymmetric one; hence, the symmetric product of the poling fields, $(E_x^0 H_y^0 + E_y^0 H_x^0)$, governs the poling and not their cross product. This also means that the magnetically induced polarization counterrotates with the magnetic field. Since neither component of the ME susceptibility changes sign below T_N [4], we concluded that the symmetric part dominates the low-temperature ME tensor. As a result, the magnitudes of the traceless symmetric

TABLE I. Summary of the magnetic excitations in terms of exciting fields, optical directional anisotropy (ODA), and classification of the resonances. This table is based on the zero-field measurements shown in Fig. 3.

Mode	Excitation	Remanent ODA	Class
1	$\mathbf{H}^\omega \parallel x, \mathbf{E}^\omega \parallel y$	+ODA (small)	ME resonance
2	$\mathbf{H}^\omega \parallel z$	no ODA	magnon
3	$\mathbf{H}^\omega \parallel x, \mathbf{E}^\omega \parallel y$	−ODA (large)	ME resonance
4	$\mathbf{H}^\omega \parallel z$	no ODA	magnon
5	$\mathbf{H}^\omega \parallel z$	no ODA	magnon
6	$\mathbf{H}^\omega \parallel x$	+ODA (100%)	ME resonance
7	$\mathbf{E}^\omega \parallel z$	no ODA	electromagnon
8	$\mathbf{E}^\omega \parallel x$	no ODA	electromagnon
9	$\mathbf{H}^\omega \parallel x$	−ODA (100%)	ME resonance
10	$\mathbf{H}^\omega \parallel z$	no ODA	magnon
11,12,13	present in each polarization	ODA	character cannot be determined

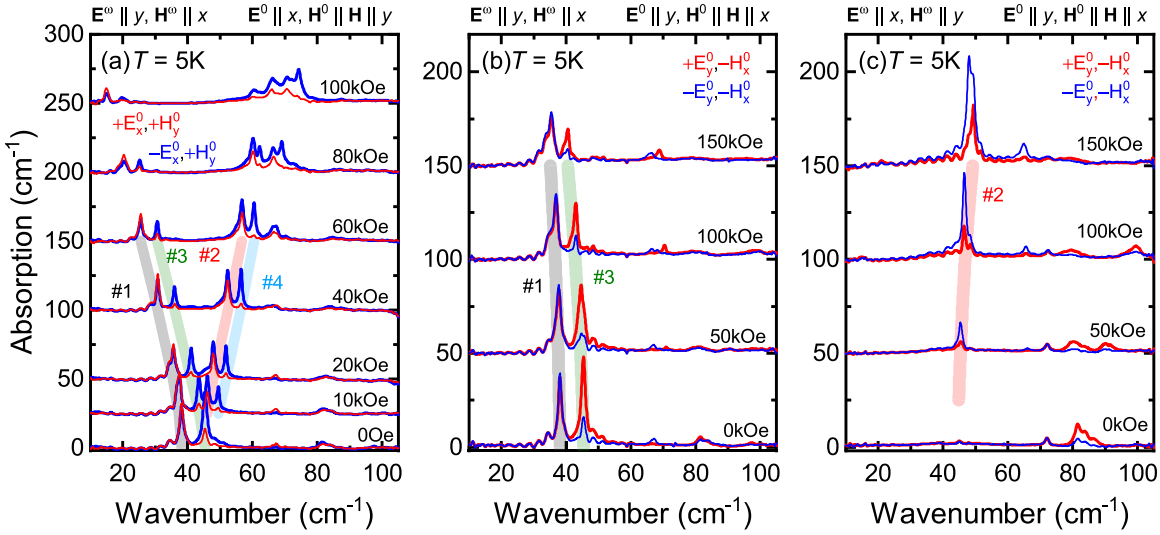

FIG. 4. Magnetic field dependence of the optical absorption spectra measured at $T = 5$ K for different combinations of the poling fields. The reference spectra, taken in the paramagnetic phase ($T = 30$ K), were subtracted from the spectra measured at $T = 5$ K. The poling fields were applied in the (a) ($\mathbf{E}^0 \parallel x$, $\mathbf{H}^0 \parallel y$) and (b) and (c) ($\mathbf{E}^0 \parallel y$, $\mathbf{H}^0 \parallel x$) configurations; the static magnetic field applied after poling was $\mathbf{H} \parallel \mathbf{H}^0$. The $\mathbf{E}^\omega$ polarization of the electromagnetic radiation was set along the (a) and (b) y and (c) x axes. For the purpose of clarity, each spectrum is shifted in proportion to the applied field by (a) 25 cm^{-1}/10 kOe and (b) and (c) 10 cm^{-1}/10 kOe.

and antisymmetric components of the static ME susceptibility are estimated to be $\chi^{\text{symm}}/c = 23.5$ ps/m and $\chi^{\text{antisymm}}/c = 8.5$ ps/m, respectively, based on the static measurements. The symmetric part is about 2.8 times larger than the antisymmetric one.

The selection rules were further studied by recoding the absorption spectra with light polarized along all the principal axes. The results of this systematic study are summarized in Fig. 3(a) and in Table I. In total, 13 resonances are observed, one more than expected from the multiboson spin-wave theory of a four-sublattice AFM with $S = 3/2$ spins [13]. Since the structural symmetry is preserved, no new phonon modes are expected in the magnetically ordered phase; thus, the origin of the extra mode is unclear. Figure 3(b) schematically illustrates the character of the different excitations. In the case of the usual zone-center magnon modes of antiferromagnets, there is a finite $\mathbf{H}^\omega$-induced magnetization in each unit cell, as the different magnetic sublattices oscillate in phase. There may be a dynamic electric polarization associated with the presence of individual spins, but these local polarizations oscillate out of phase and average to zero over the unit cell. Thus, these modes couple to only uniform $\mathbf{H}^\omega$ and not $\mathbf{E}^\omega$. In contrast for an electromagnon (E-magnon), responding only to $\mathbf{E}^\omega$, there is a finite electric polarization of the unit cell induced by the spin dynamics, but the dynamic magnetization is canceled due to the out-of-phase oscillation of the different sublattices. In the case of ME resonances, both the dynamic magnetization and polarization of the unit cell are finite; thus, these modes can be excited by $\mathbf{H}^\omega$ as well as $\mathbf{E}^\omega$. Modes 2 and 4 are usual magnon modes which are excited only by the oscillating magnetic field of light [13]. Modes 1, 3, 6, and 9 are ME resonances, as they exhibit ODA and are excited by both the H_x^ω and E_y^ω components of light. Mode 8 is an E-magnon, as it is excited only by E_x^ω. Modes 11–13 do not show simple selection rules but appear simultaneously for any polarization of the light, and they exhibit ODA for H_y^ω; thus, they are ME resonances. In summary, four magnon modes are excited by H_z^ω (2, 4, 5, and 10), four ME resonances are excited by H_x^ω as well as E_y^ω (1, 3, 6, and 9), and two E-magnons are excited by E_z^ω and E_x^ω (7 and 8, respectively).

VI. FIELD DEPENDENCE OF THE SPIN-WAVE EXCITATIONS

The characters and the frequencies of the spin-wave excitations together with their dynamic ME effect are further investigated using the magnetic-field-dependent absorption measurements shown in Fig. 4. The magnetic field dependence of the absorption spectra, measured at $T = 5$ K, is presented in Figs. 4(a) and 4(b) for $\mathbf{E}^\omega \parallel y$ and in Fig. 4(c) for $\mathbf{E}^\omega \parallel x$. The reference signal was again recorded in the paramagnetic phases at $T = 30$ K and subtracted from the $T = 5$ K spectra. The external magnetic field was applied in the same direction as the magnetic field used for poling, $H \parallel H^0$. Since the external magnetic field does not change the magnetic phase of the sample at low temperature [32], the domain state selected by the poling is preserved during the field-dependent measurements. The poling fields $E_x^0 = 1$ kV/cm and $H_y^0 = 100$ kOe are applied in Fig. 4(a). In this case, the two modes observed in zero field split into four distinct excitations. Modes 1 and 3 shift to lower energies in proportion to the magnetic field, while modes 2 and 4 shift to higher energies. In experiments corresponding to Figs. 4(b) and 4(c), poling fields of the same magnitude were applied in the perpendicular configuration, i.e., $\mathbf{E}^0 \parallel y$ and $\mathbf{H}^0 \parallel x$. In Fig. 4(b), only modes 1 and 3 are observed. With increasing magnetic field, they soften weakly and lose oscillator strength, while in Fig. 4(c) only mode 2 appears and slightly shifts to higher energies. In zero magnetic field, mode 2 is a usual magnon with no ODA; however, due to hybridization to

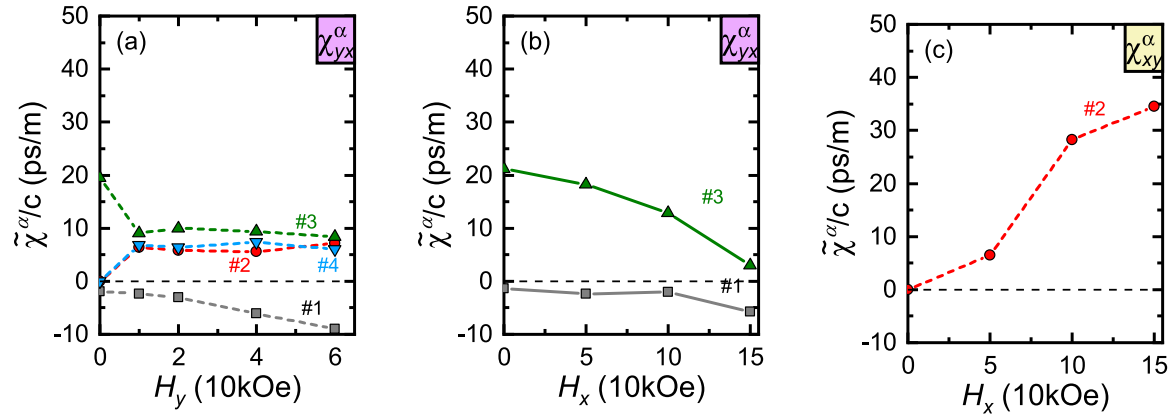

FIG. 5. Individual contributions of the different ME spin resonances to the static ME effect, calculated using the ME sum rule. (a) and (b) Field dependence of χ_{yx} for domain α, with $\mathbf{H} \parallel y$ and $\mathbf{H} \parallel x$, respectively. (c) Field dependence of χ_{xy} for domain α, with $\mathbf{H} \parallel x$. The color coding and the numbering of the curves correspond to the labeling of the modes in Fig. 4. For χ^{α}_{yx} and χ^{α}_{xy} the sum of the different contributions and their field and temperature dependences are shown in Fig. 6 in comparison with the data from the static measurements.

modes 1 and 3 it also shows considerable directional effect in finite magnetic fields.

According to the sum rule established in Ref. [21], excitations with ME character contribute to the static ME effect:

$$\chi_{ij}(0) = \frac{c}{2\pi}\int_0^{\infty} \frac{\Delta\alpha(\omega)}{\omega^2} d\omega, \tag{5}$$

where $\Delta\alpha(\omega)$ is the absorption difference caused by the ODA for light polarization $\mathbf{E}_i^{\omega}$ and $\mathbf{H}_j^{\omega}$. If the optical transitions are well separated in energy, it is possible to estimate the weight of each excitation to the static ME effect by limiting the integration around the excitation. We estimate the error of the individual contributions, originating from the weak overlap of neighboring modes, to be smaller than ± 4 ps/m. The contributions of the respective resonances for domain α are denoted as $\tilde{\chi}^{\alpha}$.

The individual contributions of modes 1–4 to the static ME susceptibility estimated from the data presented in Fig. 4(a) for $\mathbf{H}^0 \parallel y$ are shown in Fig. 5(a). In this case the polarization of light $\mathbf{E}^{\omega}$ is perpendicular to the corresponding $\mathbf{E}^0$ poling field, and likewise, $\mathbf{H}^{\omega} \perp \mathbf{H}^0$, which corresponds to the transverse ME susceptibility in the static limit. The usual magnons, modes 2 and 4, which are forbidden in zero magnetic field for the polarization E_x^{ω} and H_y^{ω}, gain optical weight as well as a finite contribution to the χ^{α}_{yx} ME susceptibility in finite fields (for further details see Fig. S4 in the Supplemental Material). For fields larger than $H = 10$ kOe, modes 2, 3, and 4 have a roughly equal and field-independent contribution to the static ME effect. In contrast to the other excitations, mode 1 has a negative and increasing contribution in larger H field.

Figures 5(b) and 5(c) show the field dependence of the $\tilde{\chi}^{\alpha}_{yx}$ and $\tilde{\chi}^{\alpha}_{xy}$ ME susceptibilities for the $\mathbf{H} \parallel x$ field in the form of individual contributions from the different modes calculated using the ME sum rule on the data in Figs. 4(b) and 4(c), respectively. Modes 1 and 3 contribute only to χ^{α}_{yx}, while χ^{α}_{xy} is dominated by mode 2. Note that the contributions to χ^{α}_{yx}

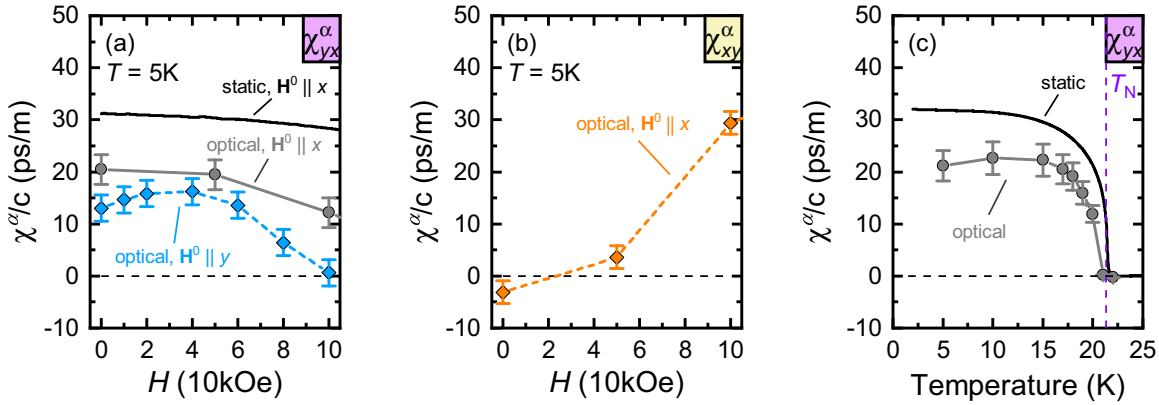

FIG. 6. (a) and (b) Magnetic field and (c) temperature dependences of the static and optical ME susceptibilities. The optical data were calculated using the ME sum rule over the complete spectral window. In (a), the gray and blue curves, corresponding to the field dependence of χ^{α}_{yx} for $\mathbf{H} \parallel x$ and $\mathbf{H} \parallel y$, respectively, should coincide at $H = 0$. Their slight deviation may come, e.g., from the imperfectness of the ME single-domain state in one of the measurements. (b) the magnetic field dependence of χ^{α}_{xy} in applied field $\mathbf{H} \parallel \mathbf{H}^0 \parallel x$. In (c), the optical spectroscopy measurements were carried out in the absence of H field, while static ME susceptibility was taken in warming runs with $H =$ 10 kOe field. The corresponding, temperature-dependent optical absorption spectra can be found in Fig. S3 [24]. The error bars were estimated using the average of the ME susceptibilities between $\pm H$ fields.

from modes 1 and 3 have opposite signs for any direction of the magnetic field.

In Fig. 6 the zero-field static ME susceptibility obtained from magnetocurrent measurements and the sum of the contributions of the studied optical modes are compared. The value obtained via the ME spectroscopy, $\chi_{yx}/c = +20.5 \pm 2.9$ ps/m, is in rather good agreement with the static value $|\chi_{yx}|/c = 32$ ps/m. In this case the observed ME resonances explain well the bulk of the static ME response; that is, the polarization is mainly induced by the spin dynamics associated with the spin-wave modes observed in our experiment. On the other hand, $\chi_{xy}/c = -3.1 \pm 2.2$ ps/m, deduced from the optical experiments, is much smaller than the ME susceptibility $|\chi_{xy}|/c = 15$ ps/m measured in the static limit. The most likely explanation for this discrepancy is the presence of additional ME mode(s) or ME electronic excitations, lying out of the limited frequency range of our THz absorption measurement.

VII. CONCLUSIONS

The antiferromagnetic $LiCoPO_4$ has two possible antiferromagnetic domain states with opposite signs of the ME coupling, which can be selected by the simultaneous application of $\mathbf{E}^0$ and $\mathbf{H}^0$ poling fields orthogonal to each other. When selecting one of the domains by ME poling, the material shows optical directional anisotropy without any external fields, where the more transparent and absorbing directions are interchanged for the two domains. Using straightforward measurements of THz optical absorption after applying different ME poling configurations, we have found that the relative sign of the two allowed static ME susceptibility terms, χ_{yx} and χ_{xy}, is the same. According to our findings, the magnetic order promotes a cross coupling between electric and magnetic degrees of freedoms, which is described by a tensor with a symmetric (quadrupolar) component larger than the antisymmetric (torroidal) component. In summary, this optical method can be utilized to determine all off-diagonal elements of the ME susceptibility in a wide range of ME materials.

ACKNOWLEDGMENTS

The authors are grateful to J. Romhányi and K. Penc for discussions and for the technical assistance provided by A. Kikkawa and M. Kriener. V.K. was supported by RIKEN Incentive Research Project FY2016. This project was supported by institutional research funding IUT23-3 of the Estonian Ministry of Education and Research, by European Regional Development Fund Project No. TK134, by the bilateral program of the Estonian and Hungarian Academies of Sciences under Contract No. NKM-47/2018, by the BME-Nanonotechnology and Materials Science FIKP grant of EMMI (BME FIKP-NAT), by Hungarian NKFIH Grant No. ANN 122879, and by the Deutsche Forschungsgemeinschaft (DFG) via the Transregional Research Collaboration TRR-80: From Electronic Correlations to Functionality (Augsburg-Munich-Stuttgart).

[1] V. M. Dubovik and V. V. Tugushev, Phys. Rep. **187**, 145 (1990).
[2] N. A. Spaldin, M. Fiebig, and M. Mostovoy, J. Phys.: Condens. Matter **20**, 434203 (2008).
[3] B. B. van Aken, J.-P. Rivera, H. Schmid, and M. Fiebig, Nature (London) **449**, 702 (2007).
[4] J.-P. Rivera, Ferroelectrics **161**, 147 (1994).
[5] M. Baum, K. Schmalzl, P. Steffens, A. Hiess, L. P. Regnault, M. Meven, P. Becker, L. Bohatý, and M. Braden, Phys. Rev. B **88**, 024414 (2013).
[6] P. Tolédano, D. D. Khalyavin, and L. C. Chapon, Phys. Rev. B **84**, 094421 (2011).
[7] P. Tolédano, M. Ackermann, L. Bohatý, P. Becker, T. Lorenz, N. Leo, and M. Fiebig, Phys. Rev. B **92**, 094431 (2015).
[8] I. Kézsmárki, N. Kida, H. Murakawa, S. Bordács, Y. Onose, and Y. Tokura, Phys. Rev. Lett. **106**, 057403 (2011).
[9] Y. Kato, K. Kimura, A. Miyake, M. Tokunaga, A. Matsuo, K. Kindo, M. Akaki, M. Hagiwara, M. Sera, T. Kimura, and Y. Motome, Phys. Rev. Lett. **118**, 107601 (2017).
[10] S. Bordács, I. Kézsmárki, D. Szaller, L. Demkó, N. Kida, H. Murakawa, Y. Onose, R. Shimano, T. Rõõm, U. Nagel, S. Miyahara, N. Furukawa, and Y. Tokura, Nat. Phys. **8**, 734 (2012).
[11] P. Borisov, A. Hochstrat, X. Chen, W. Kleemann, and C. Binek, Phys. Rev. Lett. **94**, 117203 (2005).
[12] Y. Shiratsuchi, S. Watanabe, H. Yoshida, N. Kishida, R. Nakatani, Y. Kotani, K. Toyoki, and T. Nakamura, Appl. Phys. Lett. **113**, 242404 (2018).
[13] V. Kocsis, K. Penc, T. Rõõm, U. Nagel, J. Vít, J. Romhányi, Y. Tokunaga, Y. Taguchi, Y. Tokura, I. Kézsmárki, and S. Bordács, Phys. Rev. Lett. **121**, 057601 (2018).
[14] P. Babkevich, L. Testa, K. Kimura, T. Kimura, G. S. Tucker, B. Roessli, and H. M. Rønnow, Phys. Rev. B **96**, 214436 (2017).
[15] S. Di Matteo, Y. Joly, and C. R. Natoli, Phys. Rev. B **72**, 144406 (2005).
[16] C. Ederer, Eur. Phys. J. B **71**, 349 (2009).
[17] M. Fiebig, T. Lottermoser, D. Frohlich, A. V. Goltsev, and R. V. Pisarev, Nature (London) **419**, 818 (2002).
[18] A. S. Zimmermann, B. B. Van Aken, H. Schmid, J.-P. Rivera, J. Li, D. Vaknin, and M. Fiebig, Eur. Phys. J. B **71**, 355 (2009).
[19] T. Arima, J. Phys.: Condens. Matter **20**, 434211 (2008).
[20] M. Saito, K. Taniguchi, and T. Arima, J. Phys. Soc. Jpn. **77**, 013705 (2008).
[21] D. Szaller, S. Bordács, V. Kocsis, T. Rõõm, U. Nagel, and I. Kézsmárki, Phys. Rev. B **89**, 184419 (2014).
[22] R. Santoro, D. Segal, and R. Newnham, J. Phys. Chem. Solids **27**, 1192 (1966).
[23] D. Vaknin, J. L. Zarestky, L. L. Miller, J.-P. Rivera, and H. Schmid, Phys. Rev. B **65**, 224414 (2002).
[24] See Supplemental Material at http://link.aps.org/supplemental/10.1103/PhysRevB.100.155124 for further magnetization, polarization, and optical absorption measurements, as well as for the illustration of the experimental configurations.

[25] A. Szewczyk, M. U. Gutowska, J. Wieckowski, A. Wisniewski, R. Puzniak, R. Diduszko, Y. Kharchenko, M. F. Kharchenko, and H. Schmid, Phys. Rev. B **84**, 104419 (2011).
[26] V. M. Khrustalyov, V. M. Savytsky, and M. F. Kharchenko, Low Temp. Phys. **42**, 280 (2016).
[27] A. S. Zimmermann, D. Meier, and M. Fiebig, Nat. Commun. **5**, 4796 (2014).
[28] R. Saint-Martin and S. Franger, J. Cryst. Growth **310**, 861 (2008).
[29] Y. Takahashi, R. Shimano, Y. Kaneko, H. Murakawa, and Y. Tokura, Nat. Phys. **8**, 121 (2012).
[30] F. Wooten, *Optical Properties of Solids* (Academic, New York, 1972).
[31] V. Kocsis, Ph.D. thesis, Budapest University of Technology and Economics, 2016.
[32] N. F. Kharchenko, V. M. Khrustalev, and V. N. Savitskii, Low Temp. Phys. **36**, 558 (2010).